

# Physical-mechanical behavior of alkali-activated materials produced by the one-part method based on fly ash and rice husk ash

L. F. T. Domingos<sup>1\*</sup>, A. G. S. Azevedo<sup>1</sup>, K. Strecker<sup>2</sup>

<sup>1</sup>Federal University of São João del-Rei, Department of Natural Sciences, 36301-160, São João del-Rei, MG, Brazil

<sup>2</sup>Federal University of São João del-Rei, Department of Mechanical Engineering, São João del-Rei, MG, Brazil

## Abstract

The study on the physical-mechanical properties of alkali-activated materials (AAM) produced by the 'one-part' method was carried out. For this, residues such as fly ash and rice husk ash (RHA) were used. The alkaline activator (NaOH) was calcined together with RHA for 2 h at 750 °C. Dry mixes were prepared by replacing fly ash with 10%, 20%, and 30% by weight of the calcined material. The samples produced were characterized after 7 and 28 days of curing. The results showed that the investigated variables (calcined material content and curing time at room temperature) were responsible for important variations: compressive strength from 2.40 to 24.92 MPa, modulus of elasticity from 0.90 to 12.32 GPa, water absorption from 2.92% to 13.64%, apparent porosity from 4.82% to 20.02%, and density from 1.48 to 1.71 g/cm<sup>3</sup>. It was concluded that these variations were due to the high concentration of Na<sub>2</sub>O and SiO<sub>2</sub> in the dry mixtures.

**Keywords:** alkali-activated materials, fly ash, rice husk ash, one-part method.

## INTRODUCTION


The search for alternative materials as a way to minimize the environmental impacts caused by the production and use of Portland cement in the civil construction industry has been growing nowadays more and more. According to Okoye [1], this new class of materials, also known as alkali-activated materials (AAM), should be able to replace traditional cement, ensuring high compressive strength, chemical inertness, and low cost, making it a competitive alternative to the market. AAM had its first patent published in 1908 by Hans Kúrl where, theoretically, a compound formed by an amorphous source of SiO<sub>2</sub> and Al<sub>2</sub>O<sub>3</sub> in contact with alkaline activating solutions was obtained with highly cementing properties [2]. The synthesis of AAM can be performed by alkaline activation of aluminosilicates present in calcined clays and industrial by-products [3-5]. The traditional alkaline activation methodology is based on the union of solids rich in aluminosilicates (metakaolin, fly ash, granulated blast furnace slag, among others) with metallic hydroxide solutions (NaOH and KOH) and, in some cases, silicate solutions of alkali metals (Na<sub>2</sub>SiO<sub>3</sub>) are added to the system [6].

When studies aimed at the production of AAM began to consolidate in the literature, the vast majority of the synthesis route called 'two-part' was commonly used. This methodology is based on the mixture of two components: alkaline solution(s) and aluminosilicate material(s). The alkaline solution acts as an activator for the reactive aluminosilicate, promoting its dissolution and subsequent formation of the NASH-type aluminosilicate gel (N=Na<sub>2</sub>O, A=Al<sub>2</sub>O<sub>3</sub>, S=SiO<sub>2</sub>, and H=H<sub>2</sub>O), which is responsible for the increase of the compressive strength of the hardened material.

In the work developed by Azevedo et al. [7], it was shown that the production of AAM via two-part has shown good results, especially when different types and compositions of alkaline activators (Na<sub>2</sub>O and Na<sub>2</sub>SiO<sub>3</sub>) are used. However, when used on a large scale, it should be considered that the need for preparation and handling of highly alkaline solutions requires extreme care, which represents an increase in the danger of the paste production process. In addition to the high alkaline character of the activator solutions used in this type of production, there is at the same time a decrease in the workability of the pastes due to the viscosity of the solutions (especially when using Na<sub>2</sub>SiO<sub>3</sub> or K<sub>2</sub>SiO<sub>3</sub>) [8]. A new methodology for the production of AAM is the process called 'one-part' or 'just-add-water'. This process presents itself as a promising alternative in the synthesis of AAM because it minimizes the problems related to the preparation of alkaline solution(s) when using the conventional method (two-part), and can be used to produce the AAM [8, 9]. According to Abdollahnejad [10], this mechanism is similar to the Portland cement paste production process, where only water is added to the system.

In order to promote the improvement of AAM to substantially be applied in various sectors, researchers have focused on the use of agro-industrial residues as a mechanism to improve the circular economy [11, 12]. These residues, generated by different industrial activities, are currently one of the great challenges faced by large urban centers. The agro-industrial sectors produce large amounts of liquid and solid wastes, and its inadequate disposal generates numerous environmental problems such as air, soil, and water pollution [13]. The reuse of agro-industrial residues, mineral ash such as rice husk ash (RHA) has been widely investigated by researchers due to the high silica-rich minerals. The RHA presents a high content of silica in the reactive form and can be used as pozzolanic material [14-17]. However, there is a

\*luistonholo@gmail.com

 <https://orcid.org/0000-0003-2605-1220>

lack of studies aimed at the manufacture of AAM based on rice husk ash and fly ash by the one-part method, with a view to greater acceptance of this material in the construction market as possible replacements for Portland cement. Thus, the objective of this research was to evaluate the physical-mechanical behavior of AAM produced by the one-part method using fly ash as a precursor of aluminosilicate and RHA as a source of silicon-rich component for the system.

## MATERIALS AND METHODS

**Materials. Fly ash (FA) and rice husk ash (RHA):** the fly ash used was an industrial residue produced in the thermoelectric power generation complex Jorge Lacerda located in the city of Capivari de Baixo in the state of Santa Catarina, Brazil. The RHA used as an alternative silicon-rich source came from the company Raisis Substratos Agrícolas, located in Brotas/SP, Brazil. Both materials were sieved with a 100 mesh (0.149 mm) sieve, to remove large particles and some impurities that might be present. **Alkaline activator - sodium hydroxide (NaOH):** the sodium hydroxide (R.G.) used in this work was from Sulfal Química, with 98% purity.

**Methods. Dry mix production:** for the production of the dry mixture, fly ash, RHA, and NaOH were used. First, for the production of the alkaline activator, RHA was mixed with NaOH in defined quantities based on laboratory tests, aiming at a proportion of 50% Na<sub>2</sub>O (Table I). This mixture was calcined for 2 h at 750 °C (Fig. 1) with a heating rate of 10 °C/min, using a muffle furnace (10P-S, EDG). After being calcined, it was cooled and, subsequently, ground in a planetary ball mill (PQ-N2, Across Int.), until a 100 mesh passing material was obtained. After grinding, the material produced was stored in a polypropylene plastic bag to avoid contact with H<sub>2</sub>O molecules, until the production of dry mixtures with fly ash. The dry mixtures responsible for the production of AAM were obtained by partially replacing the fly ash by different proportions in weight of calcined material (10%, 20%, and 30%), as shown in Table II. Each mixture (fly ash+calcined material) was properly stored until the production of the pastes. The different mixtures were identified by the nomenclature FA (indicating the presence of fly ash), CRA (indicating the presence of calcined rice husk ash), and the number was related to the percentage of fly ash that was replaced by the calcined material containing NaOH.

**AAM production by one-part or just-add-water:** the production of alkali-activated pastes followed the following steps. First, the dry mixtures (Table II) were homogenized in a mechanical mixer (I-3010, Contenco) for 2 min at a slow speed. Subsequently, water was added to the system with an H<sub>2</sub>O/solid ratio of 0.37 by mass and the mixture was homogenized again for 3 min until a paste was formed without the presence of agglomerated solids. After preparation, the pastes were accommodated in cylindrical plastic molds with dimensions of 50x25 mm (height x diameter) and subjected to vibration for 4 min, to a total compression in the mold and removal of air bubble [18]. Then, to prevent the loss of water through evaporation, the molds were sealed with PVC film

Table I - Composition of the calcined mixture produced with RHA and NaOH.

| Quantity of RHA (g) | Quantity of NaOH (g) | Quantity of Na <sub>2</sub> O* (g) | Na <sub>2</sub> O (wt%) |
|---------------------|----------------------|------------------------------------|-------------------------|
| 120                 | 160                  | 124                                | 50                      |

\*: in NaOH.



Figure 1: Image of RHA+NaOH after calcination at 750 °C for 2 h.

for 24 h and kept at laboratory temperature (~25 °C) until the moment of thermal curing of the samples, carried out in an oven for another 24 h at 75 °C. After thermal curing, the molds were subjected to facing on both sides, then opened; the specimens removed were then stored at room temperature until the characterization day (7 and 28 days).

**Characterization of precursor materials (fly ash and RHA) and AAM:** the mineralogical characterization of the precursor materials and geopolymers was performed using an X-ray diffractometer (XRD, Shimadzu), with a voltage of 30 kV and a current of 30 mA. The radiation used was CuKα ( $\lambda=0.15462$  nm) with a step of 0.02° and a scanning speed of 2 °/min, between 5° and 65°. The identification of the phases of the materials under study was carried out by comparing the diffraction peaks presented by the ICSD (inorganic crystal structure database) files. For morphological analysis, a scanning electron microscope (SEM, TM 3000, Hitachi) coupled with an energy dispersive spectrometer (EDS, X-Flash mim SVE, Bruker) was used. To analyze the chemical composition, an energy dispersive X-ray fluorescence spectrometer (EDX 8000, Shimadzu) was used. The compressive strength was determined by a uniaxial

Table II - Compositions of dry mixtures prepared with different contents of calcined materials.

| Dry mix | Fly ash (g) | Calcined material (g) | Na <sub>2</sub> O (g) | SiO <sub>2</sub> (g) | Na <sub>2</sub> O/SiO <sub>2</sub> <sup>#</sup> | Al <sub>2</sub> O <sub>3</sub> /SiO <sub>2</sub> <sup>#</sup> | H <sub>2</sub> O/Na <sub>2</sub> O <sup>#</sup> |
|---------|-------------|-----------------------|-----------------------|----------------------|---|---|---|
| FACRA10 | 368.18      | 40.91                 | 20.46                 | 258.47               | 0.10  | 0.26  | 23.15   |
| FACRA20 | 327.27      | 81.82                 | 40.91                 | 251.52               | 0.16  | 0.24  | 11.58   |
| FACRA30 | 286.36      | 122.73                | 61.37                 | 244.58               | 0.24  | 0.22  | 7.78  |

<sup>#</sup> molar ratio.

compression test in compliance with NBR-5739 standard [19], using a universal testing machine (AG-X plus, Shimadzu) under a crosshead speed of 3 mm/min. The data obtained were treated using a software (Trapezium X v.1.2.6, Shimadzu). The Young's modulus by longitudinal frequency was determined from a pulse of longitudinal vibration produced by an electroacoustic transducer (Pundit). The modulus of elasticity (E) was calculated in accordance with BS-1881 Part 203 [20]:

$$E = \rho \cdot V^2 \cdot \frac{(1+\nu) \cdot (1-2\nu)}{1-\nu} \quad (A)$$

where  $\rho$  is the density of the hardened state sample (kg/m<sup>3</sup>),  $V$  is the speed that an ultrasonic wave travels the specimen in the longitudinal direction (km/s), and  $\nu$  is the Poisson's ratio (0.2) [21]. Physical properties, such as density, apparent porosity, and water absorption, were determined following the instructions given in the British standard BS EN ISO 10545-3 [22], using the Archimedes principle. For this, the specimens were immersed in water and subjected to a vacuum for 24 h before obtaining the mass of the saturated samples and submerged in water with the aid of an analytical hydrostatic balance. To determine the influence of factors (calcined material content and curing time at room temperature) on the response variables (compressive strength and modulus of elasticity), an analysis of variance (ANOVA) was used. A significance level of 5% ( $p \leq 0.05$ ) was considered, which indicated that the interaction of factors significantly affected the response.

## RESULTS AND DISCUSSION

### Fly ash and RHA characterizations

*Elementary chemical composition:* the chemical compositions of the raw materials are shown in Table III. The fly ash was basically composed of silicon and aluminum, with lower concentrations of other elements and can be classified as type F because the amount of SiO<sub>2</sub>, Al<sub>2</sub>O<sub>3</sub>, and Fe<sub>2</sub>O<sub>3</sub> was greater than 70% and the content of CaO less than 10% as described by the ASTM C618 standard [23]. Rice husk ash acted as a

complementary source of silicon for the manufacturing of fly ash-based AAM with 95.79% of silica in its composition. This value was above those expected and found in the literature, which ranges from 80% to 95% [24, 25].

*Analysis of crystalline phases:* the XRD patterns of fly ash and RHA are shown in Figs. 2a and 2b, respectively. The diffractogram of fly ash showed peaks of diffraction

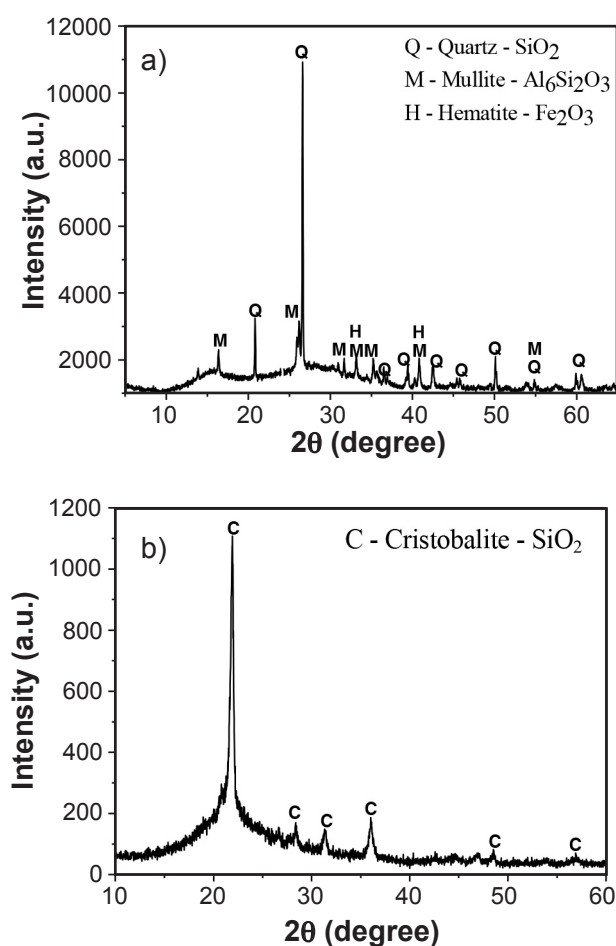


Figure 2: X-ray diffractograms for: a) fly ash; and b) RHA.

Table III - Chemical compositions (wt%) of fly ash and RHA used to produce AAM.

| Residue | SiO <sub>2</sub> | Al <sub>2</sub> O <sub>3</sub> | Fe <sub>2</sub> O <sub>3</sub> | CaO  | Other oxides      | SiO <sub>2</sub> /Al <sub>2</sub> O <sub>3</sub> <sup>#</sup> |
|---------|------------------|--------------------------------|--------------------------------|------|-------------------|---|
| Fly ash | 64.88            | 31.23                          | 3.88                           | 2.99 | 0.35 <sup>a</sup> | 2.07  |
| RHA     | 95.79            | 1.05                           | 0.33                           | 1.02 | 1.81 <sup>b</sup> | 91.05   |

<sup>#</sup> molar ratio; <sup>a</sup> ZnO, MnO, Cr<sub>2</sub>O<sub>3</sub>, SrO, CuO, Rb<sub>2</sub>O, Y<sub>2</sub>O<sub>3</sub>, PbO, Ga<sub>2</sub>O<sub>3</sub>, GeO<sub>2</sub>, NiO, NbO; <sup>b</sup> K<sub>2</sub>O.

of different crystalline phases. According to Williams and Riessen [26], these are phases that arise during the burning of coal at very high temperatures (1200-1600 °C) and in a highly oxidizing environment. Diffraction peaks corresponding to crystalline phases of quartz ( $\text{SiO}_2$ ), mullite ( $\text{Al}_6\text{Si}_2\text{O}_{13}$ ), and hematite ( $\text{Fe}_2\text{O}_3$ ) were also identified by Belmokhtar *et al.* [27]. The diffractogram also showed a halo between  $10^\circ$  and  $40^\circ$  ( $2\theta$ ), which indicated the presence of amorphous material; the vast majority of the amorphous (reactive) aluminosilicates reacts during the activation of the ash after the contact with the alkaline solutions. The diffractogram of RHA (Fig. 2b) also had characteristics of an amorphous material, due to the presence of a halo between  $15^\circ$  and  $40^\circ$  ( $2\theta$ ). The characteristic crystalline peaks of cristobalite ( $\text{SiO}_2$ ), a form of free silica (together with quartz and tridymite), were observed, similar to that found by Cordeiro *et al.* [28], who reported that its presence is an indication that the burning of the RHA was carried out at a high temperature ( $\sim 950^\circ\text{C}$ ) for a prolonged combustion time. It should be noted, in this regard, that the burning temperature and time are important factors that define the content of amorphous silica or crystalline phases present in the RHA.

*Analysis of morphology and surface chemical composition:* SEM images of fly ash and RHA with different magnifications are shown in Fig. 3. The micrographs of fly ash (Figs. 3a and 3b) showed spherical particles of varying diameters and clusters of spheres of random sizes, scattered over each other. A study [29] reports that these spheres can be hollow (cenospheres) or contain other spheres of smaller diameter inside them (plerospheres), as can be seen in Fig. 4. Figs. 3c and 3d show the morphology observed in the RHA. It is possible to verify that the particles were long and contorted in shape, which, according to Amick [30], was caused by the burning process. Fig. 3c, in particular, shows in greater detail the presence of the internal and external epidermis of one of the rice husk particles present in the ash. The external epidermis, with a wavy characteristic, concentrates the highest percentage of silica. The internal epidermis, with its cellular and porous structure, is known as the 'silica skeleton', resulting from the removal of lignin and cellulose during burning. The silica present in the ash is concentrated mainly within the external epidermis, towards the middle of the shell structure. However, a small but significant amount of silica resides within the internal epidermis, adjacent to the grain of rice [31].

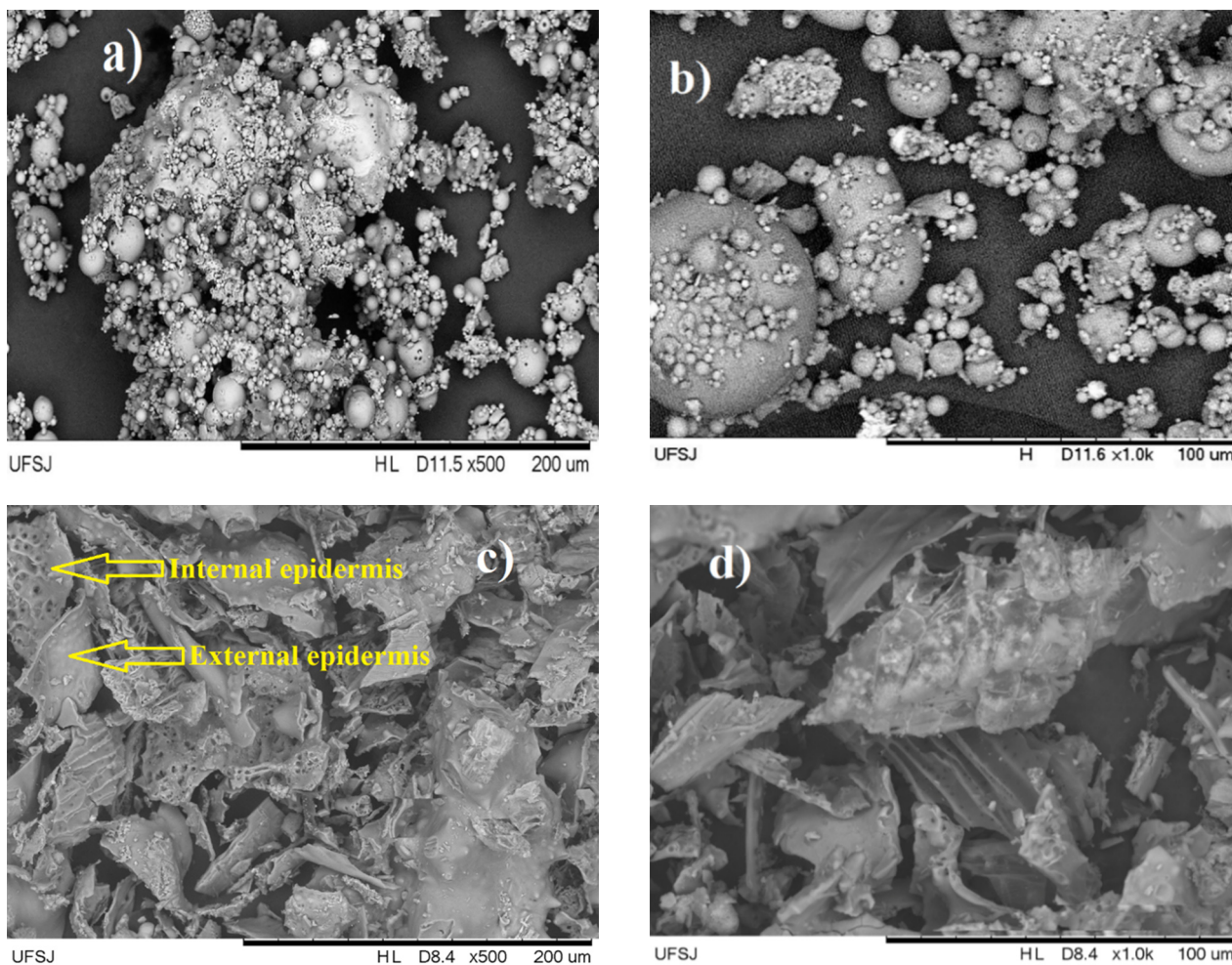


Figure 3: SEM micrographs of fly ash (a,b) and RHA (c,d) at different magnifications

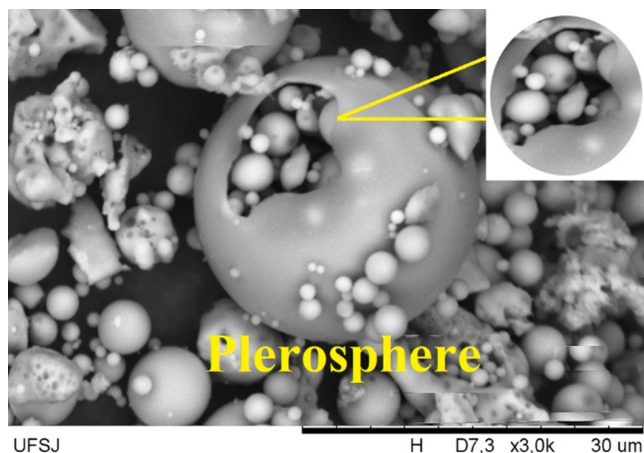


Figure 4: SEM micrograph of fly ash showing of a plerosphere.

To more accurately assess the properties of fly ash and RHA, as well as their chemical compositions, analyzes were carried out by EDS (energy dispersive spectroscopy). The Quantax 70 program was used and different areas were selected (Figs. 5a and 5b) in order to quantify the main oxides present in the samples. The results of the analysis

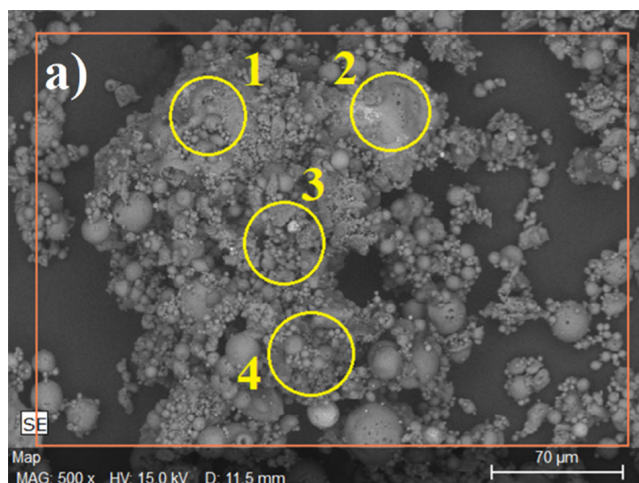


Figure 5: SEM micrographs showing areas selected for EDS analysis: a) fly ash; and b) RHA.

Table IV - Oxide contents (wt%) present in different areas indicated in Fig. 5 for fly ash and RHA.

| Area    | SiO <sub>2</sub> | Al <sub>2</sub> O <sub>3</sub> | Fe <sub>2</sub> O <sub>3</sub> | CaO     |
|---------|------------------|--------------------------------|--------------------------------|---------|
| Fly ash |                  |                                |                                |         |
| 1       | 62.21            | 25.52                          | 10.31                          | 1.96    |
| 2       | 55.13            | 24.50                          | 17.97                          | 2.40    |
| 3       | 57.50            | 23.31                          | 16.66                          | 2.53    |
| 4       | 66.26            | 27.22                          | 4.02                           | 2.50    |
| Average | 60.3±5.0         | 25.1±1.7                       | 12.2±6.4                       | 2.3±0.3 |
| RHA     |                  |                                |                                |         |
| 1       | 90.88            | 3.40                           | 4.32                           | 1.40    |
| 2       | 98.98            | 0.21                           | 0.37                           | 0.08    |
| 3       | 99.11            | 0.43                           | 0.01                           | 0.45    |
| 4       | 98.02            | 0.46                           | 0.48                           | 1.03    |
| Average | 96.7±3.9         | 1.1±1.5                        | 1.3±2.0                        | 0.7±0.6 |

by EDS presented in Table IV make us understand that, since it is a superficial and punctual analysis, there were small differences in the values when compared with the X-ray fluorescence technique (Table III), which provides a composition as a whole. However, it is possible to ratify that the classification of fly ash used for the development of this work is type F, complying with ASTM C618 [23].

#### *Characterization of AAM produced by the one-part method*

**Compressive strength:** Fig. 6a shows values related to the compressive strength for the AAM produced from the substitution of fly ash by different proportions of CRA, after 7 and 28 days of curing at room temperature. According to the results obtained, it was possible to verify an increase in the compressive strength as the proportion of CRA in relation to fly ash increased. The specimens manufactured with 10% by weight of CRA (FACRA10) showed considerably low values (close to 3.9 MPa), even after 28 days of curing. This is related to an insufficient amount of alkali for the formation of the N-A-S-H gel (N=Na<sub>2</sub>O, A=Al<sub>2</sub>O<sub>3</sub>, S=SiO<sub>2</sub>, and H=H<sub>2</sub>O), which is mainly responsible for increasing the compressive strength of the AAM [32]. After adding 30% by weight of CRA, the specimens showed a maximum compressive strength close to 24.9 MPa after 7 days, representing an increase close to 90% in comparison with specimens manufactured with 10% by weight of CRA. This value was also higher than the values found by others [6, 33], even after 28 days of ambient cure. This increase may be associated with a greater amount of Na<sub>2</sub>O and SiO<sub>2</sub> in the system, resulting from the replacement of fly ash by the prepared dry mixture. The increase in species such as Na<sub>2</sub>O and SiO<sub>2</sub> favors the dissolution and polymerization of a greater number of fly ash particles. According to Apolonio et al. [12] and Liew et al. [34], the increase in compressive

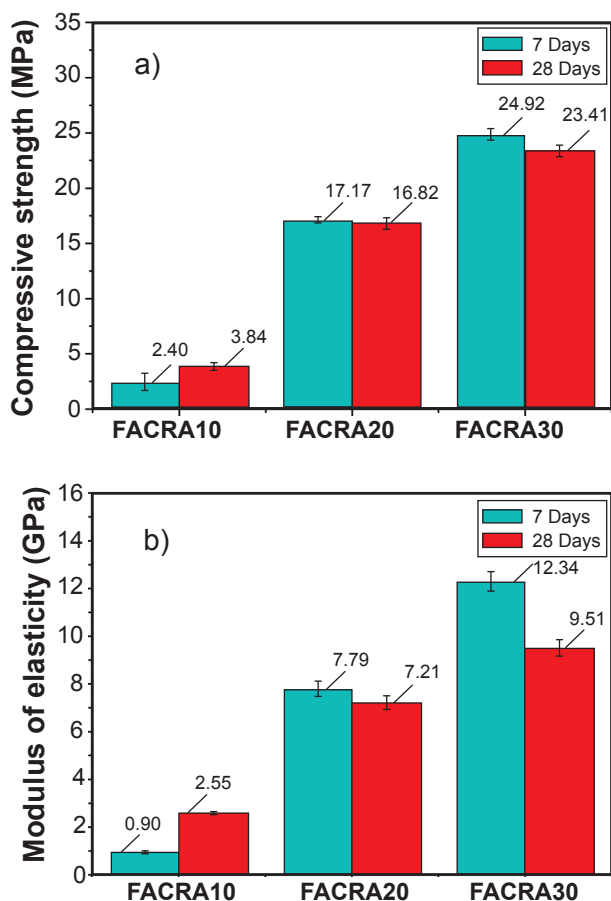


Figure 6: Graphs of uniaxial compressive strength (a) and elastic modulus (b) of AAM manufactured samples by substituting fly ash for different proportions of CRA, after different times of room temperature curing.

strength is associated with the greater dissolution of aluminosilicates with the later formation of N-A-S-H gel in the hardened specimens. The greater amount of  $\text{Na}_2\text{O}$  promotes an increase in the alkalinity of the system after adding water. The increase in pH favors a greater dissolution of the amorphous particles present in the aluminosilicate material, which are more susceptible to forming the AAM [6, 8, 35, 36].

It was also possible to observe small reductions in compressive strength values with the increase in the proportion of CRA after 28 days of ambient cure. According to Soutsos *et al.* [37], this reduction is associated with the excess of  $\text{OH}^-$  ions in the NaOH used to obtain the dry mixture involving RHA+NaOH. This excess of  $\text{OH}^-$  ions in the system causes the precipitation of aluminosilicates that promote the reduction of the polymer chains formed and, therefore, decrease the compressive strength of the material. This phenomenon is the same observed in the production of AAM by the two-part, reinforcing the idea that obtaining the inorganic binder is similar in both processes. This slight reduction in compressive strength after certain ambient curing times was also observed by Sturm *et al.* [17], who carried out the preparation of geopolymers by the one-part

method using rice husk ash and  $\text{NaAlO}_2$  (as an alkaline activator and complementary source of  $\text{Al}_2\text{O}_3$  and  $\text{Na}_2\text{O}$ ), showing that after 7 days of room temperature curing the specimens had reduction behavior in terms of compressive strength.

Table V shows the results of the analysis of variance for the compressive strength results. It can be affirmed that the interaction between the investigated factors (the content of CRA and time of room temperature curing) significantly influenced the strength values, 95% confidence or higher (p-value of 0.000). The adjusted (adj)  $R^2$  value (99.67%) indicated that the analysis model adopted for the compressive strength results was satisfactory, as the closer to 1 (or 100%), the more reliable the statistical data.

Table V - Results of analysis of variance for the compressive strength values.

| Anova (one-way)                        | p-value ( $\leq 0.05$ ) |
|--|-------------------------|
| Response variable                      | Compressive strength    |
| Main factors: CRA content, curing time | 0.000                   |
| Adj $R^2$ (%)                          | 99.67                   |

*Modulus of elasticity by longitudinal frequency:* the results of Young's modulus are shown in Fig. 6b. This modulus was determined using a non-destructive method that relates the modulus to the speed of ultrasound wave propagation in the specimen. There was an increase in the values of the elastic modulus as greater proportions of CRA were used to make the specimens. The highest value obtained, 12.3 GPa, was for specimens produced with 30% by weight of CRA in relation to fly ash (FACRA30), maintained for 7 days in room temperature curing. It was also noted that, after 28 days, the FACRA20 and FACRA30 samples showed a reduction in their results. This phenomenon was related to what was observed in the analysis of uniaxial compressive strength, where the excess of  $\text{OH}^-$  ions can promote the precipitation of aluminosilicates, causing the decrease of the formed polymer chains and, consequently, of the values of compressive strength and modulus of elasticity. The values of modulus of elasticity are correlated with the values of compressive strength [38]. Therefore, it is important to make an analogy of the averages of the values of the elastic modulus obtained with the ultrasonic speed verified in each specimen during the analysis. Table VI numerically shows that the speed at which the ultrasonic wave traveled the specimen in the longitudinal direction was directly proportional to the amount of CRA used to manufacture the AAM. This was because, as previously described, the increase in contents of species such as  $\text{Na}_2\text{O}$  and  $\text{SiO}_2$  favored the activation of a greater number of fly ash particles. In turn, this led to the formation of materials with more solid materials and fewer defects (pores, cracks, etc.). The study developed by Silva and Campiteli [39] reports that in materials with higher mass densities, the propagation speed of the ultrasonic wave is higher and, consequently, the wave propagation time

Table VI - Average results of ultrasonic wave propagation speed, modulus of elasticity (E) by longitudinal frequency, and their respective analysis of variance.

| Sample  | Velocity (km/s) |               | E (GPa)        |               | Anova (one-way)<br>p-value ( $\leq 0.05$ ) |
|---------|-----------------|---------------|----------------|---------------|--|
|         | 7 days          | 28 days       | 7 days         | 28 days       |  |
| FACRA10 | 0.8 $\pm$ 0.0   | 1.4 $\pm$ 0.0 | 0.9 $\pm$ 0.1  | 2.6 $\pm$ 0.1 | 0.000<br>R <sup>2</sup> (adj)=91.30%       |
| FACRA20 | 2.2 $\pm$ 0.0   | 2.1 $\pm$ 0.0 | 7.8 $\pm$ 0.3  | 7.2 $\pm$ 0.3 |  |
| FACRA30 | 2.7 $\pm$ 0.1   | 2.4 $\pm$ 0.0 | 12.3 $\pm$ 0.4 | 9.5 $\pm$ 0.4 |  |

is shorter, thus increasing the modulus of elasticity. The reverse process occurs for materials that have defects, of any type, in their microstructure, as discussed previously. The results of the analysis of variance shown in Table VI allowed us to state that there was a difference between the measures evaluated, with a p-value  $\leq 0.05$ . The response obtained for adjusted R<sup>2</sup> was close to 100%, indicating that the statistical analysis adopted for the results of elastic modulus was satisfactory.

*Analysis of physical properties (water absorption, apparent porosity, and density).* *Water absorption:* Fig. 7 presents comparative results for AAM manufactured by substituting fly ash, with different proportions of CRA and room temperature curing times. It was possible to observe that the samples manufactured by substituting fly ash for 10% by weight of CRA (FACRA10) were those with the highest water absorption values, close to 13.6% and 9.4% for 7 and 28 days of cure, respectively. For samples represented by FACRA20 and FACRA30, it was possible to verify a decrease in the absorption values of H<sub>2</sub>O molecules. This fact may be associated with higher concentrations of Na<sub>2</sub>O and SiO<sub>2</sub> in the system, which benefited the formation of greater amounts of N-A-S-H gel and, consequently, the formation of a structure with fewer pores and flaws (due to the greater dissolution promoted by the alkaline environment). For Azevedo and Strecker [36], the interference of the Na<sub>2</sub>O and SiO<sub>2</sub> concentration on the water absorption may be related to the excess of

NaOH in these samples, which, after the end of the alkali activation reactions, can accumulate in the existing pores in the structure, preventing the entry of water molecules. In the work of Jindal *et al.* [40], the authors state that a lower water absorption value indicates limited pore connectivity and reduced porosity in AAM. The higher RHA content can give the material microstructural densification, decreasing the microfine pores, promoting an increase in the aluminosilicate gel, which results in an increase in the binding properties.

For FACRA20 and FACRA30 samples, after 28 days of ambient polymerization, it was possible to observe a slight increase in water absorption values. This phenomenon occurred in a similar way, for example, to that observed for the uniaxial compressive strength, where the excess of OH<sup>-</sup> ions present in the system can result in the precipitation of aluminosilicates, promoting a reduction of the polymer chains formed and, therefore, causing the possible formation of micro-faults, which can compromise the physical and mechanical integrity of the material. This can be confirmed by the decrease in the ultrasonic pulse velocity, as presented in Fig. 6b. This decrease was related to the presence of cracks and pores in the structure. The presence of these defects can promote high water absorption.

*Apparent porosity and density:* the results for apparent porosity and density of the specimens produced with different proportions of calcined material (CRA) are shown in Table VII. The apparent porosity results showed a behavior similar to that observed with respect to water absorption (Fig. 7). The samples that showed the greatest amount of pores were those made with 10% by weight of CRA (FACRA10), reaching values close to 13.8% after 28 days of curing. After the replacement of fly ash by 30% by weight of CRA (FACRA30), it was possible to observe a decrease in porosity to values close to 6.5%, representing a decrease of 53.4%. The decrease in the porosity may be related to the increase in the compressive strength and modulus of elasticity of AAM. This decrease in the number of pores may be associated with the increase in the formation of the three-dimensional structure (N-A-S-H gel) when there is an increase in the concentration of Na<sub>2</sub>O and SiO<sub>2</sub> in dry mixtures. The increase in the concentration of Na<sub>2</sub>O causes an increase in the pH values of the system, which favors the greater dissolution of the amorphous structure present in fly ash and calcined material. The greater dissolution of amorphous aluminosilicates favors a greater concentration

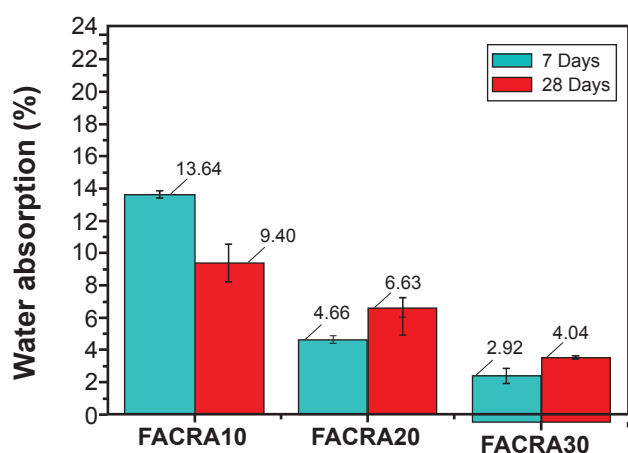


Figure 7: Water absorption of AAM manufactured samples by replacing fly ash with different proportions of CRA, after different times of room temperature curing.

Table VII - Apparent porosity and density of the samples produced with different proportions of calcined material (CRA) after different times of room temperature curing.

| Sample  | Apparent porosity (%) |            | Density (g/cm <sup>3</sup> ) |           |
|---------|-----------------------|------------|------------------------------|-----------|
|         | 7 days                | 28 days    | 7 days                       | 28 days   |
| FACRA10 | 20.02±0.28            | 13.85±1.43 | 1.48±0.00                    | 1.51±0.03 |
| FACRA20 | 7.58±0.37             | 10.54±0.83 | 1.66±0.01                    | 1.59±0.01 |
| FACRA30 | 4.82±0.71             | 6.48±0.11  | 1.71±0.01                    | 1.62±0.01 |

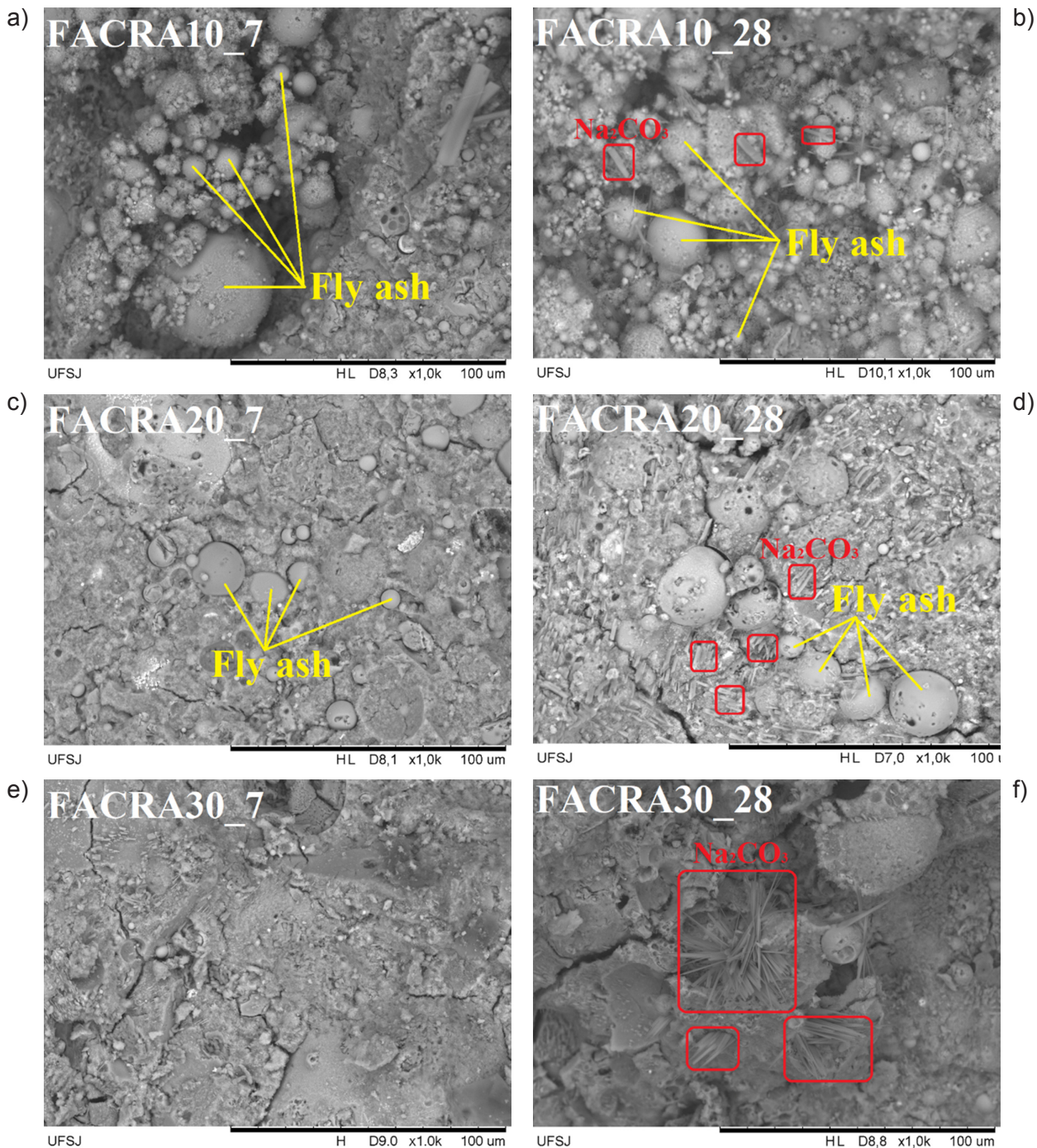


Figure 8: SEM micrographs of the surface of the specimens produced in different proportions of CRA (10%, 20%, and 30%) at different times of room temperature cure (7 and 28 days).



of species, rich in silicon and aluminum in the system, which come together to form AAM through polycondensation reactions [7, 34].

The density values of the AAM showed a small variability from 1.4 to 1.7 g/cm<sup>3</sup>, being below the calculated values (using pycnometer data) for the original fly ash of 2.06 g/cm<sup>3</sup>. This demonstrated that the partial replacement of fly ash by different proportions of CRA can promote the dissolution of the most densified aluminosilicates and the subsequent formation of AAM. The study of Mohammed et al. [41], when developing AAM using the one-part method, using fly ash and different proportions of Na<sub>2</sub>SiO<sub>3</sub> in ‘pellets’, obtained density results close to those shown in Table VII (on average 2.1 g/cm<sup>3</sup>). The authors also affirm that the presence of microstructurally denser materials and, consequently, less porous, may favor the increase of the mechanical properties of the material due to the filling of empty spaces. Based on the results, it is also possible to highlight that the increase in the Na<sub>2</sub>O and SiO<sub>2</sub> species in the system, in addition to causing an increase in compressive strength and modulus of elasticity, decreases porosity and induces the formation of materials with more densified structures, as clearly observed by the microstructures exposed by SEM.

**Morphology and surface chemical composition:** Fig. 8 shows the images of the surface of the specimens produced in different proportions of CRA (10%, 20%, and 30%) and different times of ambient cure (7 and 28 days). It was possible to observe that the samples prepared with 10% by weight of CRA (FACRA10) presented intact fly ash particles, even after 28 days of curing. This fact may be associated with the insufficient amount of Na<sub>2</sub>O present in the system. According to Azevedo and Strecker [36], this can cause a low effectiveness reaction and, consequently, the low formation of the N-A-S-H gel. In a work developed by Azevedo and Strecker [6], the authors state that intact fly ash particles even after the production of AAM pastes can, after the hardening of the structure, promote deterioration reactions with the formed N-A-S-H chain and cause defective regions in the material, compromising negatively its physical and mechanical properties. As the proportion of CRA increased (FACRA20 and FACRA30), the presence of a denser morphology with fewer fly ash particles was notorious. This occurred with the increase in the amount of alkali in the medium, making the environment more alkaline, increasing the rate of dissolution of the aluminosilicate particles (fly ash), and maximizing the alkali activation reactions. This dissolution may be related, for example, to the increase in compressive strength values, in addition to the decrease in the amount of pores present in the microstructure of the material as mentioned in the physical tests.

The increase in the ambient curing time is a predominantly important factor as it demonstrates that the dissolution reactions of the fly ash particles continue to occur, at a slower speed, even after the removal of the specimens from the oven at 75 °C. In fact, this favors the alkali activation process, in addition to inducing the formation of new phases on the surface of the materials.

In the samples identified by FACRA10\_28, FACRA20\_28, and FACRA30\_28, these new pointed phases were better visualized (surrounded by a red line, Fig. 8) and became even more evident as the proportion of CRA increased. In the literature, it is mentioned that these products result from the carbonation reaction of excess alkali that did not react during the alkaline activation of the aluminosilicate material for the production of inorganic binders [25]. Through energy dispersive spectroscopy (EDS) coupled to SEM, and using the Quantax 70 program, a superficial chemical analysis of the main elements was performed in order to assist in the process of identifying the Na<sub>2</sub>CO<sub>3</sub> crystals formed in the microstructure of the material. Fig. 9 shows an SEM image with superimposed elemental dot map layers for the surface of the FACRA30\_28 sample, which was more evident in the formation of these crystals, allowing the identification of the marked presence of sodium and carbon. It was possible to observe that in the regions where the crystals were present, there was a higher concentration of sodium

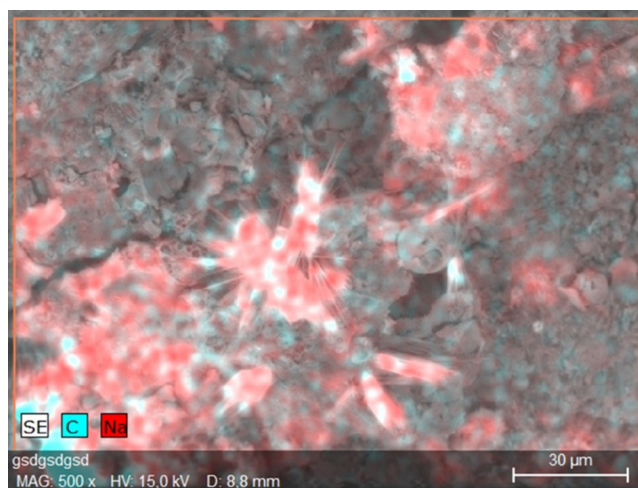


Figure 9: SEM image with superimposed elemental dot map layers (sodium and carbon) of the FACRA30\_28 sample.

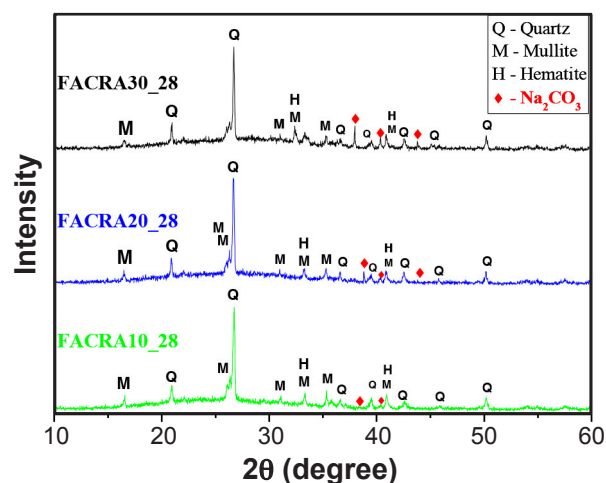


Figure 10: X-ray diffractograms for the samples FACRA10\_28, FACRA20\_28, and FACRA30\_28.

and carbon elements, demonstrating that the ambient curing time promoted the reaction of the excess of alkali with the carbon dioxide (CO<sub>2</sub>) present in the atmosphere, causing the migration of these species to the surface of the AAM.

The presence of crystals in the microstructure of samples FACRA10\_28, FACRA20\_28, and FACRA30\_28 was confirmed by XRD analysis (Fig. 10). The crystalline peaks that characterize the presence of Na<sub>2</sub>CO<sub>3</sub> were more evident as higher proportions of CRA were used after 28 days of room temperature cure. For the FACRA10\_28 sample, low-intensity peaks located at 37.9° and 40.42° (2θ) were observed. For FACRA20\_28 and FACRA30\_28, there were more intense peaks at 37.9° and 40.42° in addition to the appearance of a new peak at 43.79° (2θ). These values were close to those observed by Tchakouté *et al.* [25], namely, 37.81°, 39.84°, and 44.95° (2θ).

## CONCLUSIONS

The production of alkali-activated materials (AAM) using the one-part methodology showed promising results. The calcination process involving RHA+NaOH resulted in the formation of a powder that, in contact with water, generated an alkaline medium. As the fly ash was replaced by higher proportions of calcined material, there was an increase in the alkalinity of the system, which promoted changes in the mechanical, physical, and morphological properties of the materials after the respective days of ambient curing. Specimens produced from the replacement of fly ash by 10% by weight of the calcined product, for example, did not show such significant results, since the amount of alkali (Na<sub>2</sub>O) in the system was insufficient, which caused less formation of the N-A-S-H gel. SEM analysis showed the presence of intact fly ash particles that did not react during the alkali activation process, tending to decrease with increasing alkali concentration and curing time. It was also possible to observe the formation of crystalline structures characterized by the formation of Na<sub>2</sub>CO<sub>3</sub> crystals, due to the reaction process between the alkaline activator (which did not react during the alkali activation process) and atmospheric CO<sub>2</sub>. The AAM produced by one-part or just-add-water has the potential to be worked on a large scale and without presenting a potential health risk during their preparation, unlike those manufactured by conventional methodology, known as two-part' geopolymers. The reuse and application of solid residues such as fly ash and RHA can contribute to the reduction of soil contamination, in addition to favoring the production of alternative materials for civil construction.

## ACKNOWLEDGMENTS

This work was developed with the support of the financing agency CAPES (Coordenação de Aperfeiçoamento de Pessoal de Nível Superior), Universidade Federal de São João del-Rei (UFSJ), Complexo Termelétrico Jorge Lacerda, and Rasis Substratos Agrícolas Ltda.

## REFERENCES

- [1] F.N. Okoye, *Mater. Today Proc.* **4** (2017) 5599.
- [2] H. Kürli, "Slag cement and process of making the same", US Patent, 900939 (1908).
- [3] T. Bakharev, *Cem. Concr. Res.* **6** (2005) 1233.
- [4] A.D. Hounsi, G.L. Lecomte-Nana, G. Djétéli, P. Blanchart, *Constr. Build. Mater.* **42** (2013) 105.
- [5] X. Liu, N.A. Zhang, H. Sun, J. Zhang, L. Li, *Cem. Concr. Res.* **41** (2011) 847.
- [6] A.G.S. Azevedo, K. Strecker, *Constr. Build. Mater.* **269** (2021) 121306.
- [7] A.G. de S. Azevedo, K. Strecker, A.G. de Araújo Jr., C.A. da Silva, *Cerâmica* **63**, 366 (2017) 143.
- [8] M. Askarian, Z. Tao, G. Adam, B. Samali, *Constr. Build. Mater.* **186** (2018) 330.
- [9] A. Hajimohammadi, J.L. Provis, J.S.J. van Deventer, *Ind. Eng. Chem. Res.* **47** (2008) 9396.
- [10] Z. Abdollahnejad, "Development of foam one-part geopolymers", Dr. Thesis, Un. Minho, Portugal (2016).
- [11] D.G. Nair, K.S. Jagadish, A. Fraaij, *Cem. Concr. Res.* **36** (2006) 1062.
- [12] P.H. Apolonio, J.S. Lima, E.P. Marinho, A.C.V. Nobrega, J.C.O. Freitas, A.E. Martinelli, *Cerâmica* **66**, 378 (2020) 172.
- [13] I.M.T. Bezerra, J. Souza, J.B.Q. de Carvalho, G.A. Neves, *Rev. Bras. Eng. Agríc. Amb.* **15** (2011) 639.
- [14] K. Kaur, J. Singh, M. Kaur, *Constr. Build. Mater.* **169** (2018) 188.
- [15] M.O. de Paula, I.F.F. Tinôco, C.S. Rodrigues, E.N. da Silva, C.F. Souza, *Rev. Bras. Eng. Agríc. Amb.* **13** (2009) 353.
- [16] S.K. Das, J. Mishra, S.K. Singh, S.M. Mustakim, A. Patel, S.K. Das, U. Behera, *Mater. Today Proc.* **33** (2020) 5162.
- [17] P. Sturm, G.J.G. Gluth, H.J.H. Brouwers, H.C. Kühne, *Constr. Build. Mater.* **124** (2016) 961.
- [18] NBR 5738, "Concreto: procedimento para moldagem e cura de corpos de prova", ABNT, Brazil (2015).
- [19] NBR 5739, "Concreto: ensaio de compressão de corpos de prova cilíndricos", ABNT, Brazil (2007).
- [20] BS 1881 Part 203, "Recommendations for measurement of velocity of ultrasonic pulses in concrete", United Kingdom (1986).
- [21] T.H. Panzera, A.L. Christoforo, J.C.C. Rubio, C.R. Brown, P.H.R. Borges, L.J. Silva, *Int. J. Appl. Ceram. Technol.* **10** (2013) 474.
- [22] BS EN ISO 10545-3 Part 3, "Determination of water absorption, apparent porosity, apparent relative density and bulk density", United Kingdom (1997).
- [23] ASTM C618, "Standard specification for coal fly ash and raw or calcined natural pozzolan for use as a mineral admixture in concrete", Am. Soc. Test. Mater., USA (2010).
- [24] J. He, Y. Jie, J. Zhang, Y. Yu, G. Zhang, *Cem. Concr. Compos.* **37** (2013) 108.
- [25] H.K. Tchakouté, C.H. Rüscher, S. Kong, E. Kamseu, C. Leonelli, *Constr. Build. Mater.* **114** (2016) 276.

- [26] R.P. Williams, A.V. Riessen, *Fuel* **89** (2010) 3683.
- [27] N. Belmokhtar, M. Ammari, J. Brigui, L. Ben Allal, *Constr. Build. Mater.* **146** (2017) 621.
- [28] L.N.P. Cordeiro, A.B. Masuero, D.C.C. Dal Molin, *Matéria* **19** (2014) 150.
- [29] X. Guo, H. Shi, W.A. Dick, *Cem. Concr. Compos.* **32** (2010) 142.
- [30] J.A. Amick, *J. Electrochem.* **129** (1982) 864.
- [31] J. James, M.S. Rao, *Thermochem. Acta* **97** (1986) 329.
- [32] S.K. Nath, S. Maitra, S. Mukherjee, S. Kumar, *Constr. Build. Mater.* **111** (2016) 758.
- [33] A.F. Lopes, C.D.M. Nickel, G. Scaratti, A. Rossi, M.H. Araújo, A.N. Júnior, *J. Clean. Prod.* **273** (2020) 122917.
- [34] Y.M. Liew, C.Y. Heah, A.B. Mohd Mustafa, H. Kamarudin, *Prog. Mater. Sci.* **83** (2016) 595.
- [35] K.H. Yang, J.K. Song, A.F. Ashour, E.T. Lee, *Constr. Build. Mater.* **22** (2008) 1981.
- [36] A.G.S. Azevedo, K. Strecker, *Ceram. Int.* **43** (2017) 9012.
- [37] M. Soutsos, A.P. Boyle, R. Vinai, A. Hadjierakleous, S.J. Barnett, *Constr. Build. Mater.* **110** (2016) 355.
- [38] A.I. Marques, J. Morais, C. Santos, P. Morais, M.R. Veiga, C. Santos, P. Candeias, J.G. Ferreira, *Constr. Build. Mater.* **232** (2020) 117216.
- [39] N.G. Silva, V.S. Campiteli, *Amb. Constr.* **8** (2008) 21.
- [40] B.B. Jindal, P. Jangra, A. Garg, *Mater. Today* **32** (2020) 871.
- [41] B.S. Mohammed, S. Haruna, M.M.A. Wahab, M.S. Liew, A. Haruna, *Heliyon* **5** (2019) e02255.
- (*Rec.* 11/07/2021, *Rev.* 15/09/2021, 29/10/2021, *Ac.* 04/11/2021)

